pH-Dependent Photoinduced Electron Transfer at C_{60}-EDTA Langmuir−Blodgett Film Modified ITO Electrode

Wen Zhang, Yaru Shi, Liangbing Gan,* Chunhui Huang,* Hongxia Luo, Dengguo Wu, and Nanqiang Li

State Key Laboratory of Rare Earth Materials Chemistry and Applications, Department of Chemistry, Peking University, Beijing 100871, P. R. China

Received: August 4, 1998; In Final Form: November 3, 1998

The monolayer and multilayer films of an amphiphilic C_{60}-EDTA (C_{60}EA) and its tetramethyl ester (C_{60}EM) were fabricated on semiconducting transparent ITO electrodes by the Langmuir−Blodgett (LB) technique. The photoelectric response of the modified electrodes was measured under various conditions to explore possible mechanisms of the electron transfer in this light harvesting and conversion system. The action spectrum of photocurrent implicates the excited C_{60}EA or C_{60}EM as the photoactive species in the photoinduced electron transfer process. Anodic or cathodic photocurrent could be observed depending on the composition and concentration of redox agents in the solution and/or bias voltage applied. These results suggest that electron flow in either direction is energetically possible in the present photoelectric chemical cell. When the pH in the solution was changed, the photocurrent of C_{60}EA changed not only in its magnitude but also in its direction. Efficient photoinduced electron transfer was observed in the anodic direction. The quantum yields for the photocurrent generation of C_{60}EM and C_{60}EA monolayer−ITO system are 4.80% and 3.80% under favorable conditions.

Introduction

In the past few years the photochemical and photophysical properties of C_{60} and its functionalized derivatives have gained extensive attention as they exhibit a variety of interesting excited state properties.[1−9] Electron transfer from various electron donors[2] and semiconductor colloids[3] to photoexcited triplet C_{60} has been reported. The study of C_{60} derivatives with photo-/electroinactive substituents has revealed that intersystem crossing to the energetically lower excited triplet state exhibits a deceleration when the number of functionalizing groups is increased,[1] whereas C_{60} derivatives with photo-/electroactive substituents, such as porphyrin-,[4] ruthenium complex-,[5] carotenoid polyenes-,[6] and aniline-C_{60} diads,[7] exhibit ultrafast intramolecular electron transport. In the electron transfer process, the excited singlet state of C_{60} plays an important role. However, compared with the photophysics of fullerenes in solution, the investigation on the photophysical properties of fullerene thin films is limited. Although some effort has been made to investigate the photoactivity and photoconductivity of polycrystalline C_{60} thin films,[8] the nature of fullerene excited state in a closely packed film is still not well understood.[9]

The application of fullerenes photoactivity is mainly concerned with its strong electron-accepting capacities. Photoinduced electron transfer from conjugated polymers to C_{60} has been reported in a polymer and C_{60} heterojunction device.[10] The C_{60} moiety has been found to operate as a photosensitive unit undergoing rapid intramolecular electron transfer reaction in C_{60} ferrocene-based donor-bridge−acceptor dyads.[11] The introduction of hydrophilic groups into highly hydrophobic C_{60} made it possible to form stable C_{60}-containing LB film. A few reports have recently appeared on the formation of stable monolayer and multilayer films from amphiphilic C_{60} derivatives.[12] Such well-organized molecular assemblies are an essential requirement for the construction of fullerene-based nanostructured devices. It has been reported that aggregates formed in Langmuir film at the air−water interface possessed photophysical properties that are significantly different from monomers.[13]

Here we report monolayer and multilayer modified semiconductor ITO electrodes with amphiphilic C_{60}-EDTA derivatives by LB technique and the investigation of photodriven electron transfer at the electrode−electrolyte interface. Dependence of the electron transport on some factors that may enhance, decrease, or even redirect the observed photocurrents was investigated. A possible mechanism for the electron transfer process is proposed.

Experimental Section

Materials and Sample Preparation. C_{60}EM was prepared by the photochemical reaction between C_{60} and EDTA tetramethyl esters (Scheme 1) as reported.[14] C_{60}EA was prepared by the hydrolysis of C_{60}EM by a procedure similar to Hirsch's method.[15] The detailed preparation of C_{60}EA will be published separately. Methyl viologen diiodide (MV^{2+}) was synthesized by the reaction of 4,4′-bipyridyl with excess methyl iodine in refluxing ethanol for 6 h and then recrystalized from ethanol. Hydroquinone (H_2Q) and ascorbic acid (AA) were reagent grade chemicals and recrystallized from water before use. Chloroform and DMSO were purified by distillation. Deionized water purified by passing through an EASY pure RF compact ultrapure water system (Barnstead Co. US) was used in all experiments.

LB Film Preparation. Monolayer of C_{60}EM or C_{60}EA was obtained on a NIMA 622 computer-controlled Langmuir trough (UK). The air−water interface was thoroughly cleaned by complete barrier movement (surface area changed from 1200 to 80 cm^2 and the surface pressure changed by less than 0.1

10.1021/jp983315y CCC: $18.00
Published on Web 01/08/1999

SCHEME 1. Preparation and Chemical Structure of C_{60}EM and C_{60}EA

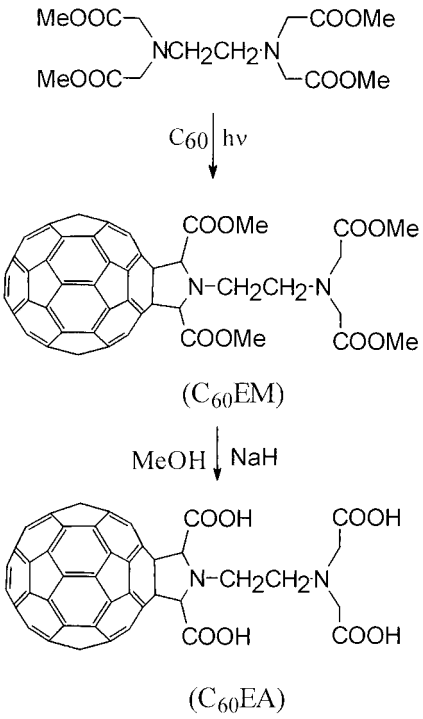

mN/m). The subphase was deionized water (20 ± 1 °C, pH 5.6, >18 MΩ·cm) or 1×10^{-3} M $CdBr_2$ solution. Spreading solutions of C_{60}EM were prepared by dissolving a small amount of the sample in chloroform to get a concentration of 1.32×10^{-4} M (solution A); A was diluted with chloroform to get a concentration of 3.96×10^{-5} M (solution B) and 1.32×10^{-5} M (solution C). Spreading solution of C_{60}EA was prepared by dissolving it in DMSO (9.9×10^{-4} M) and then diluted with chloroform to get a concentration of 1.98×10^{-5} M. An accurate amount of the above solution was carefully deposited on the clean subphase in about 1 h. After the evaporation of the solvent over 30 min, the floating films were compressed at a rate of 40 cm^2/min and the surface pressure−area ($\pi-A$) isotherm was recorded. The monolayer was deposited onto the hydrophilic pretreated transparent indium−tin oxide (ITO) glass substrate or quartz plate at a rate of 5 mm/min (vertical dipping) under a constant surface pressure of 20 or 15 mN/m for a subphase containing $CdBr_2$. Typical transfer ratios were 0.95 ± 0.05.

Photoelectrochemical and Electrochemical Measurements. The photocurrent measurements were carried out on a model 600 voltammetric analyzer (CH Instruments Inc., USA) and using a 500 W xenon lamp (Ushio Electric, Japan) as the light source. A series of filters (Toshiba, Japan) with certain bandpasses were used to obtain different wavelengths of incident light. The intensity of incident light was measured by a power and energy meter (Scientech 372, Boulder CO). The IR light was filtered throughout the experiment with a Toshiba IRA-25s filter (Japan). A three-electrode cell having a flat window for illumination of the working electrode was used. The counter electrode was Pt wire and the reference was a saturated calomel electrode. 0.1 M KCl solution was used as the electrolyte solution. All experiments were carried out under nitrogen atmosphere.

Cyclic voltammetry was measured on an EG/G PAR-273 potentiostat/galvanostat with model 270 electrochemical software. A three-electrode configuration was used throughout. The measurement in solution was carried out by using a microdisk gold electrode (27 μm diameter) as the working electrode. The counter and reference electrodes were a platinum wire and a Ag/AgCl, respectively. The concentration of C_{60} or C_{60}EM was 0.5 mM. The measurement of LB films of C_{60}-EDTA derivatives was carried out by fabricating them on ITO electrodes which were used as working electrode (effective area 0.38 cm^2) and the counter and reference electrodes were the same as mentioned above. The ferrocene/ferrocenium couple (F_C/F_C^+) was used in all electrochemical experiment as the internal standard. All measurements were performed at ambient temperature under nitrogen atmosphere in a 0.1 M acetonitrile/toluene or acetonitrile solution of $(n\text{-Bu})_4NClO_4$.

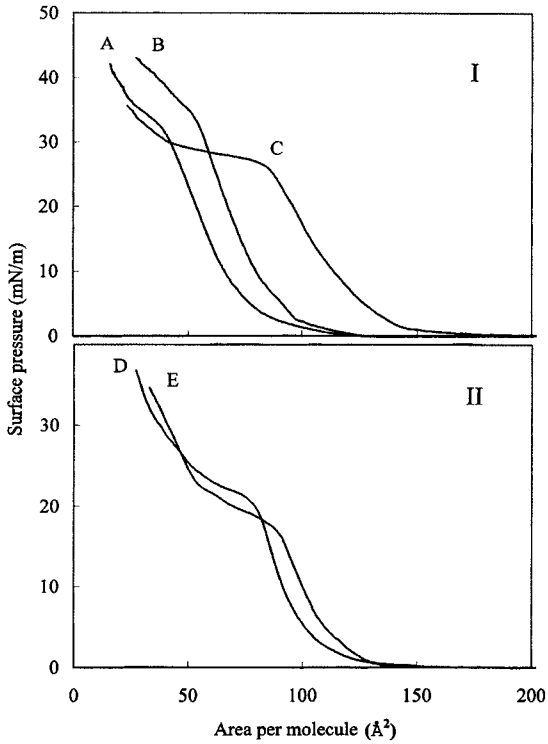

Figure 1. Surface pressure−area isotherms of C_{60}EM (I) and C_{60}EA (II) at the air/water interface, 293 ± 1 K, pH 5.6. (I): IA, solution A, 1.32×10^{-4} M; IB, solution B, 3.96×10^{-5} M; IC, solution C, 1.32×10^{-5} M. (II): IID, 1.98×10^{-5} M, subphase pH 5.6; IIE, 1.98×10^{-5}, subphase 1×10^{-3} M $CdBr_2$.

Results and Discussion

Formation of Langmuir−Blodgett Film. The surface pressure *v*s area ($\pi-A$) isotherms of the Langmuir films of C_{60}EM are different when different concentrations of spreading solutions were used. A typical result is shown in Figure 1 (I). When a relatively concentrated solution A was used, a multilayer $\pi-A$ isotherm (curve A) was obtained. The limiting area per molecule, obtained by extrapolation of the rising portion of the isotherm to $\pi = 0$, was 75 $Å^2$/molecule. The $\pi-A$ curve IB in Figure 1 was obtained by using diluted solution B and the limiting area was 88 $Å^2$/molecule. Compared with the monolayer area per molecule for other C_{60} derivatives (~100 $Å^2$/molecule),[12] it is still small, indicating a multilayer or partial multilayer film was obtained. The monolayer of C_{60}EM was obtained by using the more diluted solution C. The limiting area was 125 $Å^2$/molecule Figure 1(IC). This value is larger than that of $C_{60}O$,[16] suggesting that the substituent group of C_{60}EM occupied a certain area on the monolayers. A possible arrangement of the molecules at the air−water interface is shown in Scheme 2A. The monolayer is stable and reproducible after

SCHEME 2. Possible Packing Arrangement of C_{60}EM (A) and C_{60}EA (B) on the Air/Water Interface

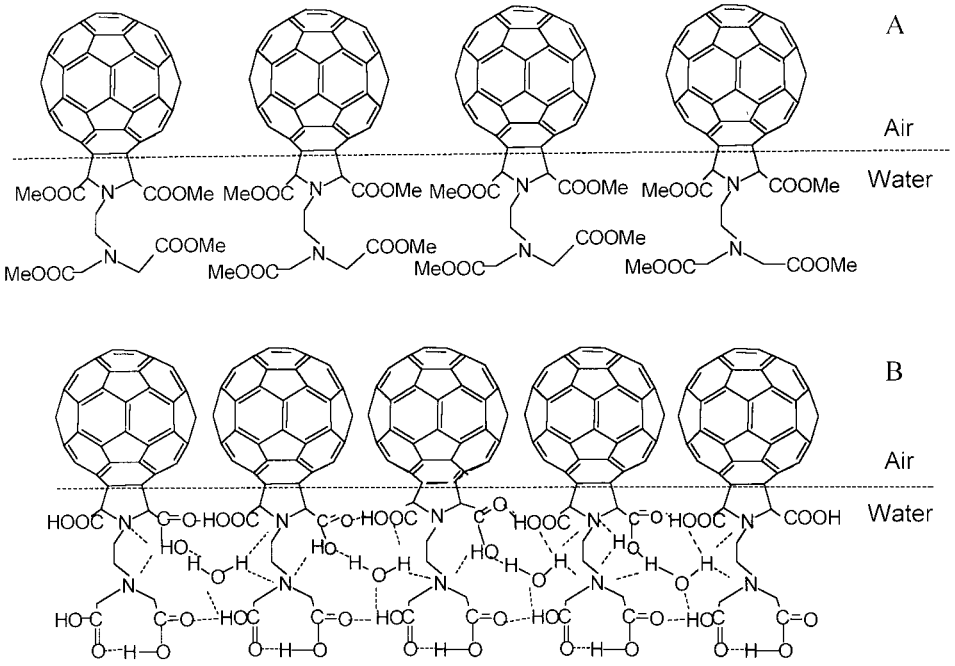

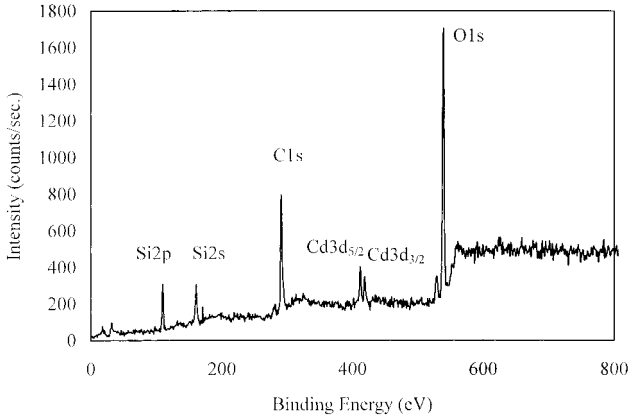

Figure 2. XPS spectrum of the C_{60}EA monolayer film on glass plate deposited from $CdBr_2$ subphase (1.0×10^{-3} M).

three times of expansion and recompression within the range of 20 mN/m.

C_{60}EA also shows good film forming properties. Its $\pi-A$ isotherm is shown in Figure 1(II). This curve is independent of the concentration of spreading solution within the range of 10^{-5} M. The limiting molecular area is 102 Å^2/molecule (Figure 1, IID). This value is smaller than that of the ester precursor C_{60}EM. Replacement of the four methyl groups and intra- and intermolecular hydrogen bonds may be responsible for the decrease of the observed limiting area (Scheme 2B). When $CdBr_2$ solution was used as the subphase, the limiting area became larger for C_{60}EA (Figure 1, IIE; 115 Å^2/molecule). This might result from the interaction between the carboxyls of C_{60}EA and Cd^{2+} in the subphase. The XPS spectrum in Figure 2 shows the presence of Cd^{2+} in a monolayer film of C_{60}EA deposited from $CdBr_2$ solution subphase.

The monolayer films of both C_{60}EM and C_{60}EA have a lower collapse pressure than most other C_{60} derivatives.[17] When the surface pressure exceeded the collapse pressure, a transfer process from monolayer to multilayer film can be clearly observed from the $\pi-A$ isotherms.

The monolayer films of both C_{60}EM and C_{60}EA could be easily transferred onto a hydrophilic quartz or ITO plate by the vertical dipping method with transfer ratios of 0.95 ± 0.05. The multilayer was transferred in Z type at the surface pressure of 20.0 ± 0.1 mN/m with a dipping speed of 5 mm/min. When the number of layers exceeds 7, the transfer ratio begins to decrease.

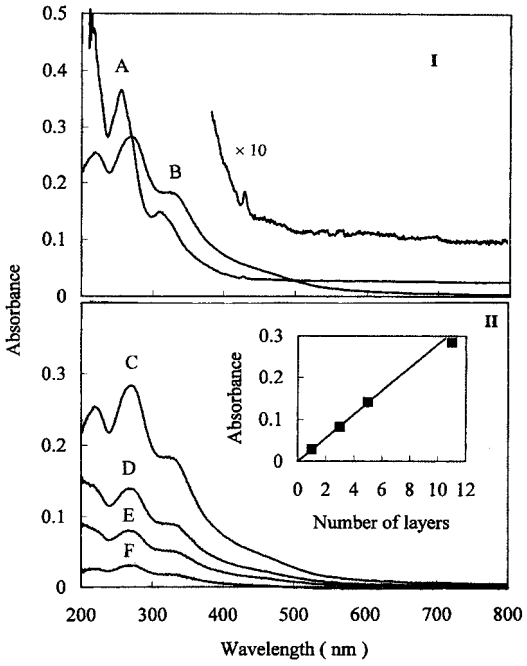

Figure 3. Electronic absorption spectra of C_{60}EM. (I): IA, *n*-hexane solution; IB, 11-layer LB film. (II): IIF, one-layer LB film; IIE, three-layer film; IID, five-layer film; IIC, 11-layer film on quartz plate.

Absorption Spectra. The UV−vis spectrum of LB film on quartz plate was recorded on a Shimadzu UV-3100 spectrophotometer. The spectra for C_{60}EM and C_{60}EA are similar. Figure 3 gives the spectra of C_{60}EM in *n*-hexane and on quartz plates. In the solution three absorptions around 254, 310, and 428 nm were found (Figure 3, IA); another band around 220 nm was not well separated from the absorption of the *n*-hexane solvent; the onset absorption lies at about 700 nm (inset in Figure 3(I)). However, in the spectrum of the C_{60}EM LB film, the 254

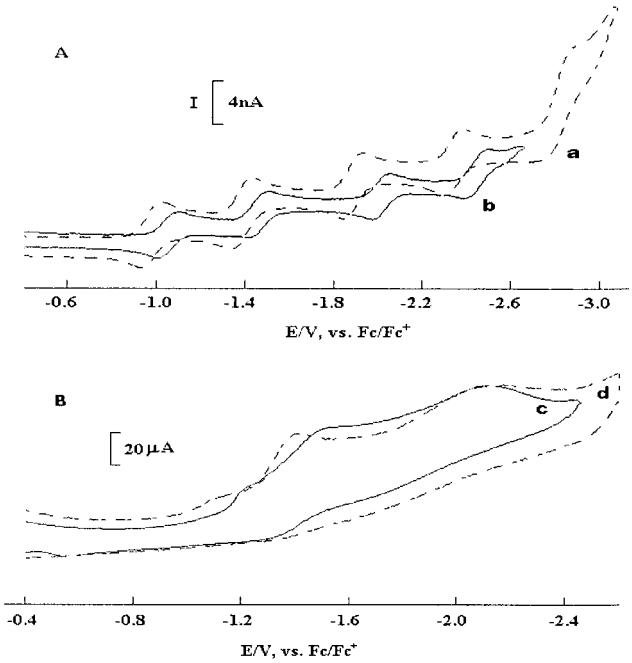

Figure 4. (A) Cyclic voltammograms of C_{60} (a) and C_{60}EM (b) at 1.0 V/s in acetonitrile/toluene + 0.1 M $(n\text{-Bu})_4NClO_4$. (B) CVs of monolayer film of C_{60}EA (c) and C_{60}EM (d) at 0.1 V/s in acetonitrile + 0.1 M $(n\text{-Bu})_4NClO_4$.

and 310 nm peaks red shift to 268 and 330 nm. The absorption at 428 nm almost disappears. These changes in the absorption are a clear indication of the electronic interaction between the C_{60} moieties of adjacent molecules.

The absorbance of C_{60}EM multilayer LB film is shown in Figure 3(II). The two main absorbances are almost the same for different layers of LB film, suggesting the interaction between C_{60} moieties mainly results from the same layer in the Z type film. The plot of the absorbance against the layer number (inset in Figure 3(II)) indicates that the Langmuir film is effectively transferred onto substrate when the number of layers is below 7.

Electrochemical Properties. Figure 4 shows the CVs of the C_{60}EM in toluene and the monolayer films of C_{60}EM and C_{60}EA on ITO electrodes. In solution C_{60}EM exhibits four well-separated reduction peaks and four corresponding reoxidation peaks. Sequential electron transfer processes are clearly observed for the four reversible reduction steps. About 80 mV negative shift of reduction potential compared with C_{60} is observed, which is consistent with other C_{60} derivatives.[18] The CV of a monolayer LB film of C_{60}EM on ITO electrode formed at the surface pressure of 20 mN/m is shown in Figure 4c. Three reduction peaks are observed with no corresponding reoxidation peaks, indicating the reduction of C_{60}EM film is irreversible. Compared with the electrochemical features of the C_{60}EM in solution, the first reduction peak of the C_{60}EM film is negatively shifted 90 mV; the second and third reduction peaks of C_{60}EM film are also a little negatively shifted; C_{60}EA monolayer films also exhibit three reduction peaks (Figure 4d). The first and second reduction peaks of C_{60}EA film are positively shifted 130 and 90 mV compared with those of the C_{60}EM film, indicating C_{60}EA is more electronegative than C_{60}EM. As in the case of C_{60}EM, no reoxidation peaks are observed. These electrochemical features of the LB films may be caused by the irreversible film damage and the hindrance of the electrons transfer in the closely packed films.The electrochemical data of C_{60}EA and C_{60}EM are summarized in Table 1.

TABLE 1: Half-Wave Potentials or Reduction Peaks of C_{60}, C_{60}EM, and C_{60}EA[a]

compd	$E^{0/-1}$	$E^{-1/-2}$	$E^{-2/-3}$	$E^{-3/-4}$
C_{60} (solution)	−0.97	−1.38	−1.88	−2.34
C_{60}EM (solution)	−1.05	−1.45	−2.01	−2.44
	−1.14[b]	−1.49[b]	−2.04[b]	−2.48[b]
C_{60}EM (LB film)	−1.23[b]	−1.50[b]	−2.11[b]	
C_{60}EA (LB film)	−1.10[b]	−1.41[b]	−2.12[b]	

[a] V vs ferrocene/ferrocenium couple. $(n\text{-Bu})_4NClO_4$ (0.1 M) in acetonitrile/toluen (1:4 v/v) or acetonitrile (films). Scan rate: 1.0 V/s (solution); 0.1 V/s (films). [b] Reduction peak positions.

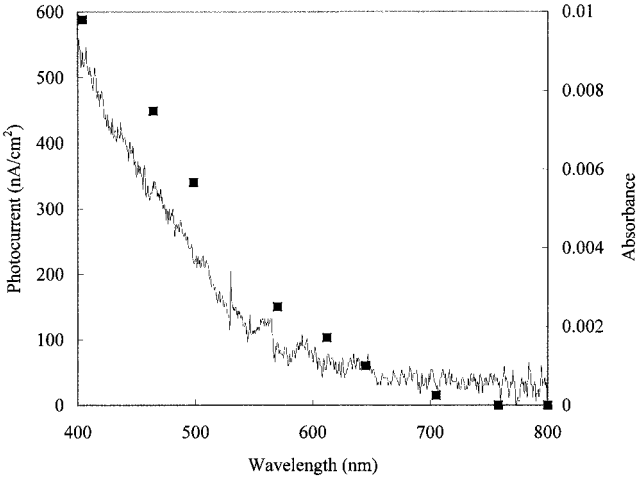

Figure 5. (■) Photocurrent action spectrum (0.1 M KCl, 17.4 mM H_2Q, pH 5.6, 0.2 V bias voltage, λ = 404 nm) and (—) absorption spectrum of a monolayer of C_{60}EM on ITO,

Photoelectric Response of the C_{60}EA and C_{60}EM Monolayers on ITO Electrodes. Since the absorbency of ITO glass increases sharply at wavelengths below 340 nm, wavelengths above 400 nm were used as the exciting source. At these wavelengths the background photocurrent of ITO glass is negligible. Figure 5 shows a typical photocurrent response as a function of excitation wavelength for the monolayer of C_{60}EM and its absorption spectrum on ITO electrode. The two spectra coincide well with each other, indicating the aggregate of C_{60}EM in the LB film is responsible for the photocurrent generation. Similar spectra were obtained for C_{60}EA on ITO electrode.

Under the illumination of 404 nm light (2.10 mW/cm^2), an anodic photocurrent (ca. 135 nA/cm^2) for C_{60}EM and a small cathodic photoelectric response (ca. 15 nA/cm^2) for the C_{60}EA−ITO system were observed, respectively. When electron donors (H_2Q or AA) or acceptor (MV^{2+}) were added to the solution, a dramatic change of photocurrent was observed not only in the magnitude but also in the direction.

The observed anodic photocurrent of C_{60}EM increases markedly with increasing H_2Q or AA concentration and reaches a limiting value at a higher concentration of H_2Q or AA (Table 2). For the C_{60}EA−ITO system, addition of H_2Q effectively reverse the photocurrent from the cathodic to anodic direction, the anodic photocurrent increases rapidly with the increase of H_2Q concentration, and levels off at 10 mM. In the presence of electron donors, especially H_2Q, the photocurrent becomes large and stable, and no decay was observed when illuminated for half an hour. For the electron acceptor MV^{2+}, an opposite effect was found. MV^{2+} suppressed the anodic photocurrent of C_{60}EM markedly and redirected the direction of the electron transfer when a large excess of MV^{2+} was added to the electrolyte. In the presence of 28 mM MV^{2+}, ca. 190 nA/cm^2 cathodic photocurrent was obtained for C_{60}EM. However, the effect of

TABLE 2: Photocurrent Density (nA/cm^2) of the Monolayer Films of C_{60}EA and C_{60}EM on ITO under Different Conditions

samples	KCl[a]	KCl, H_2Q[b]	KCl, AA[c]	KCl, MV^{2+} [d]	KCl, H_2Q, bias[e]
C_{60}EM	135	419	351	−190	666
C_{60}EA	−15	127		−39	463

[a] [KCl] = 0.1 M. [b] [H_2Q] = 17.5 mM for C_{60}EM and 10 mM for C_{60}EA. [c] [AA] = 17.6 mM. [d] [MV^{2+}] = 28 mM for C_{60}EM film and 2 mM for C_{60}EA film. [e] Bias voltage = 0.2 V, at pH 10 for C_{60}EM and pH 5.6 for C_{60}EA.

TABLE 3: Photocurrent (nA/cm^2) of C_{60}EM and C_{60}EA LB Films[a] at Different pH Values

	pH		
samples	4	7	9
C_{60}EM	110	160	182
C_{60}EA	−135	98	128

[a] A monolayer film for C_{60}EM and a five-layer film for C_{60}EA in the phosphate buffer solution containing 0.1 M KCl.

MV^{2+} on the photocurrent of C_{60}EA was not so apparent as on C_{60}EM. The photocurrent only increased from 15 to 39 nA/cm^2 when 2 mM MV^{2+} was added to the solution and was almost saturated at 39 nA/cm^2 for C_{60}EA films.

The anodic photocurrent of C_{60}EM increases as the positive bias of the electrode increases. The photocurrent is always anodic in the presence of H_2Q under potential range from −0.2 to 0.2 V vs SCE. In the case of C_{60}EA the photocurrent changes to anodic when H_2Q is added. When the bias voltage was more negative than −0.08 V vs SCE, the direction of photocurrent changes from the anodic back to cathodic even in the presence of H_2Q. The fact that both H_2Q and bias can change the direction of the photocurrent of C_{60}EA film indicates that electron flow in either direction is energetically possible.

pH-Dependent Photoinduced Electron Transfer. The pH in solution has a dramatic influence on the photocurrent of the C_{60}EA−ITO−electrolyte system. As mentioned above, H_2Q can reverse the cathodic photocurrent of C_{60}EA to anodic. When the pH of solution was below 5, the photocurrent could be changed back to cathodic even in the presence of H_2Q. This change cannot be caused by the shift of flatband potential of ITO electrode because the shift caused by the decrease of the pH is benificial for anodic photocurrent.[19] In order to study the effect of pH on the photocurrent of C_{60}EA, the photoelectric response of a five-layer C_{60}EA film on ITO was investigated in different pH phosphate buffer solutions containing 0.1 M KCl without H_2Q. Cathodic photocurrent of 135 nA/cm^2 at pH 4, anodic photocurrent of 98 nA/cm^2 at pH 7, and anodic photocurrent of 128 nA/cm^2 at pH 9 were observed (Table 3). So the direction of electron flow can be effectively controlled by the pH of the solution. For comparison the photocurrents of the monolayer films of the ester derivative C_{60}EM on ITO were determined and were always anodic in a pH range 2−12 under the same experimental conditions as those of C_{60}EA (Table 3). This indicates that the different states of carboxyls on the C_{60}EA must be resposible for the direction of the photocurrent.

Figure 6 shows the pH-dependent photocurrent of a five-layer film of C_{60}EA. EDTA can be used as a simple model for C_{60}EA to explain the observed pH dependency. It is well-known that EDTA can exist in different forms depending on the pH of the solution. At pH 4, EDTA exists almost entirely as H_2Y^{2-} (Y is EDTA anion) and gradually changes to more "basic forms" or "acidic forms" when the pH value becomes bigger or smaller.

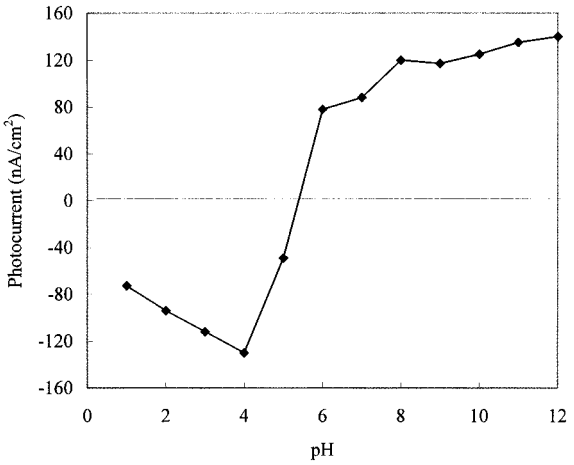

Figure 6. Photocurrent as a function of pH in solution for a five-layer film of C_{60}EA on ITO (0.1 M KCl, λ = 404 nm).

SCHEME 3. Possible Mechanism of the pH-Modulated Electron Transfer Process

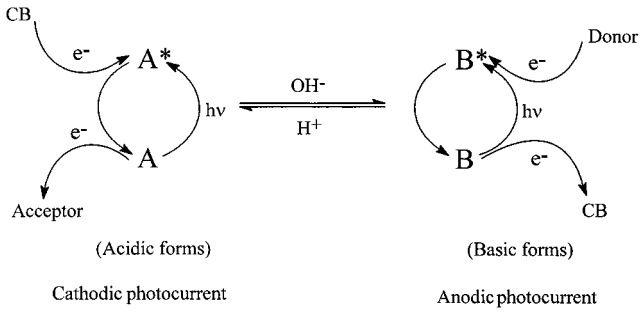

The related acid−base equilibrium for C_{60}EA is shown as follows:

$$C_{60}H_6Y^{2+} \underset{H^+}{\overset{OH^-}{\rightleftharpoons}} C_{60}H_5Y^{+} \underset{H^+}{\overset{OH^-}{\rightleftharpoons}} C_{60}H_4Y \underset{H^+}{\overset{OH^-}{\rightleftharpoons}} C_{60}H_3Y^{-} \underset{H^+}{\overset{OH^-}{\rightleftharpoons}} C_{60}H_5Y^{2-} \underset{H^+}{\overset{OH^-}{\rightleftharpoons}} C_{60}HY^{3-} \underset{H^+}{\overset{OH^-}{\rightleftharpoons}} C_{60}Y^{4-}$$

When pH increases the basic forms will gradually become dominant, and when pH decreases the acidic forms will become the main species. Dramatic changes in the photocurrent were observed in a pH range from 4 to 6. This may correspond to a change of existing forms from mainly $C_{60}H_2Y^{2-}$ to $C_{60}HY^{3-}$. Scheme 3 shows the possible pathway for the pH-modulated photocurrent generation. The acidic forms of C_{60}EA lead to the production of cathodic photocurrent, while the basic forms are responsible for the anodic photocurrent. To further understand this phenomenon, the photocurrent of the monolayer C_{60}EA−Cd film on ITO was investigated. In this film the hydrogen atoms were replaced by Cd^{2+} which is similar to a situation when C_{60}EA exists in basic forms. An anodic photocurrent ranging from 18 to 26 nA/cm^2 was observed for this system. This supports the assumption that the acid−base equilibrium of C_{60}EA is responsible for the cathodic or anodic photocurrent generation.

Using the favorable factors determined above, the quantum efficiency for photocurrent generation from C_{60}EM or C_{60}EA monolayer can be calculated by the following equation:[20]

$$\Phi_\lambda = (I_{p\lambda}/q)/(F_{abs})_\lambda \quad (1)$$

where $I_{p\lambda}$ is the photocurrent (A/cm^2) at wavelength λ, q is the elementary charge in coulombs, and $(F_{abs})_\lambda$ is the number of

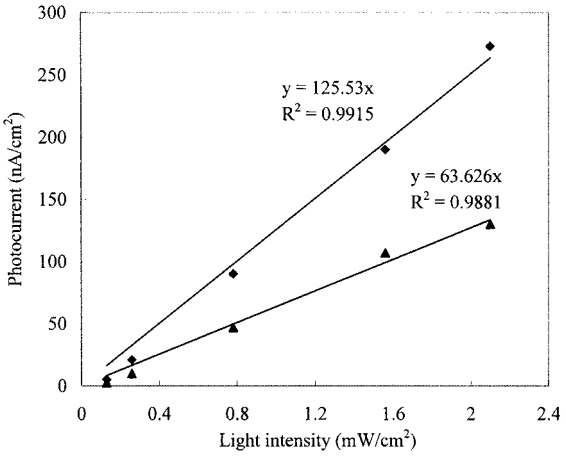

Figure 7. Photocurrent vs light intensity for the monolayers of $C_{60}EM$ (♦) and $C_{60}EA$ (▲) (0.1 M KCl, 17.4 mM H_2Q for $C_{60}EM$, and 10 mM H_2Q for $C_{60}EA$, $\lambda = 404$ nm).

photons (cm^2/s) absorbed by the film. $(F_{abs})_\lambda$ can be calculated from the number of incident photons per second, $F_{i\lambda}$, and the absorbance, A_λ, of the monolayer by eq 2:

$$(F_{abs})_\lambda = F_{i\lambda}(1 - 10^{-A\lambda}) \quad (2)$$

When the modified electrode was illuminated by monochromatic 404 nm light under 200 mV positive bias voltage, the photocurrent density was 666 nA/cm^2 in the presence of 17.4 mM H_2Q for $C_{60}EM$ at pH 10 and 463 nA/cm^2 for $C_{60}EA$ in the presence of 10 mM H_2Q at pH 5.6. The calculated quantum efficiencies are 4.80% and 3.80% respectively.

Photocurrent versus Light Intensity. The relationship between the measured photocurrent signals (i_{ph}) and the light intensity (I) can be used to judge the recombination pathway of separated charge. A good linear relationship between i_{ph} and I was obtained (Figure 7). The equation for the line can be expressed as $i_{ph} = KI^m$ [$i_{ph} = 125.53I$ (deviation coefficient $R = 0.996$) for $C_{60}EM$ and $i_{ph} = 63.63I$ ($R = 0.994$) for $C_{60}EA$]. When $m = 1$, it indicates an unimolecular recombination process.[21] Thus the data in Figure 7 shows the separated-charge loss processes in both $C_{60}EM$ and $C_{60}EA$−ITO system are a unimolecular recombination process. No saturation state of the photocurrent was observed.

Effect of LB Film Thickness. Figure 8 shows the photocurrent and quantum efficiency as a function of the layer number of $C_{60}EA$ and $C_{60}EM$ deposited on ITO electrodes. When illuminated at 404 nm (2.10 mW/cm^2), the photocurrent increases with the number of layers until it reaches a maximum at round seven layers. On the other hand, the value of the quantum efficiency exhibits a monotonic decrease with increasing number of layers for both samples.

Two factors may affect the photocurrent as the thickness of the film increases. One is the increase of photoactive molecules which may result in the enhancement of the photocurrent; another is the increase of the film's electrical resistance which may lead to a decrease of the photocurrent. The photocurrent of a seven-layer film is enhanced about 2 times for $C_{60}EM$ or 2.5 times for $C_{60}EA$ compared with the corresponding monolayer film, while the quantum efficiencies decrease about 3 times for $C_{60}EA$ and 5 times for $C_{60}EM$.

Mechanism of Photoinduced Electron Transfer. In order to examine the electron transfer process for the photocurrent generation, the energies of the relevant electronic states must be known. The reduction potentials of the excited state of $C_{60}EE$

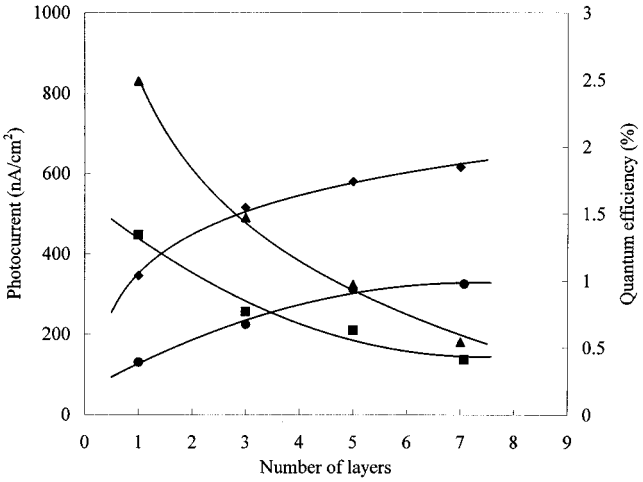

Figure 8. Dependence of the quantum efficiency [$C_{60}EM$ (▲), $C_{60}EA$ (■)] and the magnitude of photocurrent [$C_{60}EM$ (♦), $C_{60}EA$ (●)] on the number of layers (0.1 M KCl, 22 mM H_2Q for $C_{60}EA$ and 14 mM AA for $C_{60}EM$, $\lambda = 404$ nm).

($C_{60}EE$ represents both $C_{60}EA$ and $C_{60}EM$), $E°(*C_{60}EE/C_{60}EE^{\bullet-})$, are approximately given by the reduction potentials of the ground state $E°(C_{60}EE/C_{60}EE^{\bullet-})$ plus an energy term corresponding to the zero−zero spectroscopic energy of the excited state ($E_{0-0}\{C_{60}EE \rightarrow *C_{60}EE\}$).[1]

$$E°(*C_{60}EE/C_{60}EE^{\bullet-}) = E°(C_{60}EE/C_{60}EE^{\bullet-}) + E_{0-0}(C_{60}EE \rightarrow *C_{60}EE)$$

The attachment of different groups onto C_{60} leads to only minor change for the excited state energy (ca. 1.50 eV for triplet, ca. 1.77 eV for singlet).[1] The reduction potentials of $C_{60}EM/C_{60}EM^{\bullet-}$ and $C_{60}EA/C_{60}EA^{\bullet-}$ are at −1.14 V vs Fc^+/Fc (estimated from its first reduction peak) or −0.68 V vs SCE and −1.01 V vs Fc^+/Fc or −0.55 V vs SCE. Taking the energy of the C_{60} derivatives 0−0 electronic transition as 1.77 eV, the reduction potentials of the $C_{60}EM$ and $C_{60}EA$ excited singlet states, $E°(*C_{60}EM/C_{60}EM^{\bullet-})$ and $E°(*C_{60}EA/C_{60}EA^{\bullet-})$, are 1.09 and 1.22 V vs SCE, respectively. The oxidation potential of H_2Q in 0.1 M KCl solution is −0.12 V and AA is −0.21 V vs SCE. The reduction potential of MV^{2+} is −0.22 V vs SCE.[22] The energies of the conduction band (Ec) and valence band (Ev) edges of ITO can be estimated from the electron affinity of 4.4 eV, a band gap of 3.6 eV, an energy of saturated calomel electrode (SCE) *vs* vacuum of −4.75 eV, and a flatband potential at pH 7 of −4.92 eV.[19] With these data the energy level diagram in Scheme 4 can be constructed.

The anodic photocurrent may arise from a process shown below:

$$C_{60}EE \xrightarrow{h\nu} *C_{60}EE$$

$$*C_{60}EE + D \rightarrow (C_{60}EE)^{\bullet-} + D^{\bullet+}$$

$$(C_{60}EE)^{\bullet-} + (CB) \rightarrow C_{60}EE + e^-(CB)$$

where $C_{60}EE = C_{60}EM$ or $C_{60}EA$.

The $C_{60}EE$ excited state is reduced to anion by the electron donor D (AA or H_2Q). The electron transfer from the $C_{60}EE^{\bullet-}$ to the ITO electrode completes the circuit for the observed anodic photocurrent. It is well-known that C_{60} and its derivatives are good electron acceptors. In solution, the excited singlet state of fullerenes rapidly and quantitatively crosses to the long-lived

SCHEME 4. Schematic Diagram Showing Electron Transfer Processes

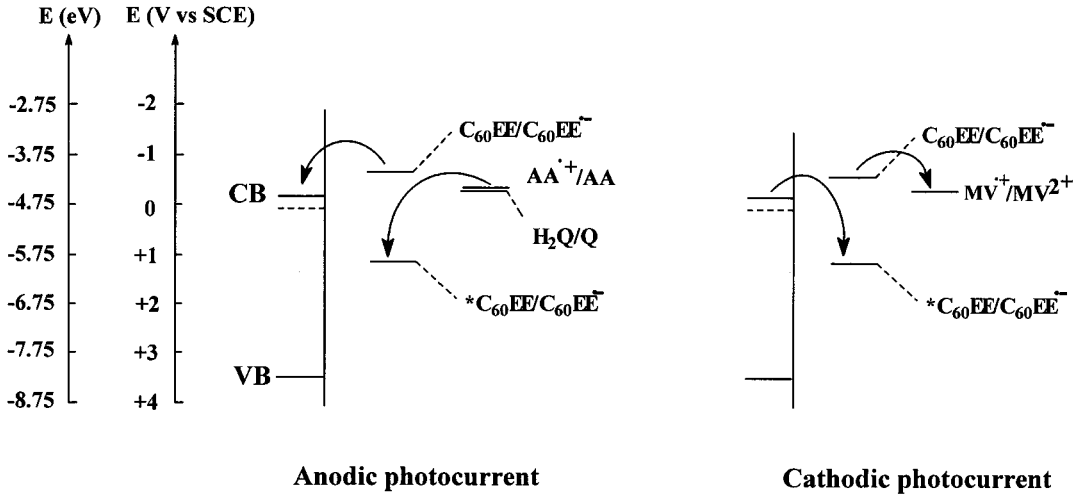

excited triplet state. The ground state quenching and triplet−triplet annihilation processes dominate the deactivation of the triplet excited state of fullerenes in solution.[1] However, in a closely packed assembly, singlet−singlet state annihilation may predominate the photophysics of the described films.

The cathodic photocurrent observed is consistent with the scheme shown below:

$$C_{60}EE \xrightarrow{h\nu} {}^*C_{60}EE$$

$${}^*C_{60}EE + (CB) \rightarrow (C_{60}EE)^{\bullet -} + (CB)^+$$

$$(C_{60}EE)^{\bullet -} + MV^{2+} \rightarrow C_{60}EE + MV^{\bullet +}$$

Electrons transfer from the conduction band (CB) of ITO to the excited state of $C_{60}EE$ leading to the formation of $C_{60}EE^{\bullet -}$, which was then oxidized by MV^{2+} regenerating $C_{60}EE$ and thus completing the circuit for the observed cathodic photocurrent. The effect of MV^{2+} on the cathodic photocurrent of $C_{60}EA$ is not as much as on the anodic photocurrent of $C_{60}EM$, indicating the coupling between the conduction band of ITO and the energy level of $C_{60}EA/C_{60}EA^{\bullet -}$ is strong and back electron donation from $C_{60}EA^{\bullet -}$ to CB strongly competes with the electron transfer to MV^{2+}.

Conclusion

Amphiphilic C_{60}−EDTA derivatives can form stable monolayer at the air−water interface and the monolayer can be deposited onto an ITO substrate. Multiple deposition to form a stack of monolayers is facile when the number of layer is below 7. The C_{60}-EDTA derivatives monolayer-sensitized semiconductor ITO electrode can initiate effective photoinduced electron transport. The photocurrent action spectrum indicates the C_{60}-EDTA derivatives as the photoactive species. The photocurrent increases as the layer number of the film increases (below seven layers). However, the quantum yield of photocurrent decreases monotonically. The direction of electron flow in the $C_{60}EA$−ITO−electrolyte system can be modulated by the pH in the solution.

Acknowledgment. The authors thank the Climbing Program (A National Fundamental Research Key Project) and the Natural Science Foundation of China for financial support (29571004 and 2967001).

References and Notes

(1) Guldi, D. M.; Asmus, K. D. J. *J. Phys. Chem. A* **1997**, *101*, 1472.

(2) (a) Arbogast, J. W.; Foote, C. S.; Kao, M. *J. Am. Chem. Soc*. **1992**, *114*, 2277. (b) Guldi, D. M.; Huie, R. E.; Neta, P.; Hungerbuhler, H.; Asmus, K.-D. *Chem. Phys. Lett*. **1994**, *223*, 511.

(3) Kamat, P. V. *J. Am. Chem. Soc*. **1991**, *113*, 9705.

(4) Kuciauskas, D.; Lin, S.; Seely, G. R.; Moore, A. L.; Gust, D. *J. Phys. Chem*. **1996**, *100*, 15926.

(5) Maggini, M.; Dono, A.; Scorrano, G.; Prato, M. *J. Chem. Soc., Chem. Commun*. **1995**, 843.

(6) Imahori, H.; Cardoso, S.; Tatman, D.; Lin, S.; Macpherson, A. N.; Noss, L.; Seely, G. R.; Sereno, L.; Chessa, de Silber. J.; Moore, T. A.; Moore, A. L.; Gust, D. *Photochem. Photobiol*. **1995**, *62*, 1009.

(7) Williams, R. M.; Zwler, J. M.; Verhoeven, J. W. *J. Am. Chem. Soc*. **1995**, *117*, 4093.

(8) Srdanov, V. I.; Lee, C. H.; Sariciftci, N. S. *Thin. Solid Films* **1995**, *257*, 233.

(9) Kazaoui, S.; Ross, R.; Minami, N. *Solid State Commun.* **1994**, *90* (10), 623.

(10) Yu, G.; Gao, J.; Hummelen, J. C.; Wudl, F.; Heeger, A. J. *Science* **1995**, *270*, 1789.

(11) Guldi, D. M.; Maggini, M.; Scorrano, G.; Prato, M. *J. Am. Chem. Soc*. **1997**, *119*, 974.

(12) (a) Vaknin, D.; Wang, J. Y.; Uphaus, R. A. *Langmuir* **1995**, *11*, 1435. (b) Ravaine, S.; Le Pecq, F.; Mingotaud, C.; Delhaes, P.; Hummelen, J. C.; Wudl, F.; Patterson, L. K. *J. Phys. Chem*. **1995**, *99*, 9551.

(13) Wang, Y. M.; Kamat, P. V.; Patterson, L. K. *J. Phys. Chem*. **1993**, *97*, 8793.

(14) Gan, L. B.; Jiang, J. F.; Zhang, W.; Su, Y.; Shi, Y. R.; Huang, C. H.; Pan, J. Q.; Lu, M. J.; Wu, Y. *J. Org. Chem*. **1998**, *63*, 4240.

(15) Lamparth, L.; Hirsch, A. *J. Chem. Soc., Chem. Commun*. **1994**, 1727.

(16) Maliszewskyj, N. C.; Heiney, P. A.; Jones, D. R.; Strongin, R. M.; Cichy, M. A.; Smith, A. B. III *Langmuir* **1993**, *9*, 1439.

(17) Zhou, D. J.; Gan, L. B.; Luo, C. P.; Tan, H. S.; Huang, C. H.; Yao, G. Q.; Zhao, X. S.; Liu, Z. F.; Xia X. H.; Zhang, P. *J. Phys. Chem*. **1996**, *100*, 3150.

(18) Suzuki, T.; Li, Q.; Khemani, K. C.; Wudl, F.; Almarsson, O. *Science* **1991**, *254*, 1186.

(19) Fromherz, F.; Arden, W. *J. Am. Chem. Soc*. **1980**, *102*, 6211.

(20) Miyasaka, T.; Watanabe, T.; Fujishima, A.; Honda, K. *J. Am. Chem. Soc*. **1978**, *100*, 6657.

(21) Donoan, K. J.; Sudiwala, R. V.; Wilson, E. G. *Mol. Cryst. Liq. Cryst*. **1991**, *194*, 337.

(22) Gratzel, M.; Moser, J. *Proc. Acad. Sci*. **1983**, *80*, 3129.